View metadata, citation and similar papers at core.ac.uk
brought to you by CORE
provided by Juelich Shared Electronic Resources

Magnetic and structural properties of GaN thin layers implanted with Mn, Cr, or V ions

V. A. Guzenko,[a] N. Thillosen, A. Dahmen, R. Calarco, and Th. Schäpers
Institute of Thin Films and Interfaces (ISG1) and CNI - Center of Nanoelectronic Systems for Information Technology, Research Centre Jülich GmbH, 52425 Jülich, Germany

L. Houben and M. Luysberg
Institute of Solid State Research (IFF) and CNI - Center of Nanoelectronic Systems for Information Technology, Research Centre Jülich GmbH, 52425 Jülich, Germany

B. Schineller and M. Heuken
AIXTRON AG, Kackertstrasse 15-17, 52072 Aachen, Germany

A. Kaluza
GLI Global Light Industries GmbH, Carl-Friedrich-Gauss-Strasse 1, 47475 Kamp-Lintfort, Germany

(Received 3 May 2004; accepted 18 August 2004)

We report on magnetic and structural properties of *n*- and *p*-type GaN layers implanted with Mn, Cr, and V. The samples were subsequently annealed in a N_2 atmosphere at a constant temperature in the range between 700 and 1050 °C. Measurements of the magnetization as a function of magnetic field as well as of the temperature show typical paramagnetic behavior. In addition, a weak antiferromagnetic coupling between the implanted ions was observed. 3d-metal rich precipitates of crystalline nature are revealed by high resolution transmission electron microscopy. © *2004 American Institute of Physics*. [DOI: 10.1063/1.1805718]

I. INTRODUCTION

Since their discovery diluted magnetic semiconductors (DMS) have attracted interest because of their potential functionalities for spintronic applications.[1] For example, a replacement of conventional ferromagnetic electrodes in a spin field effect transistor by DMS might improve spin injection efficiency due to the better matching of the materials.[2] Moreover, a local electrostatic control of magnetic moments in DMS allows concepts of designing spintronic devices.[3] Quite recently, many groups have focused on GaN-based DMS. One of the reasons is the relatively long electron spin lifetime, in comparison with GaAs.[4,5] An additional motivation is the prediction of room temperature ferromagnetism in GaN:Mn by Dietl *et al.*[6] on the basis of a mean-field Zener model, provided that a cubic GaN with simultaneously high concentration of Mn ions (~5 at.%) and valence band holes (3.5×10^{20} cm^{-3}) can be created. Successively, *ab initio* calculations by Sato and Katayama-Yoshida[7,8] based on a local spin-density approximation, which assume that Ga atoms are randomly substituted by the magnetic atoms, helped in identifying other transition metal atoms that may serve as effective magnetic dopants in GaN. They have shown that GaN:Mn is ferromagnetic up to 10% of Mn concentration, whereas for higher Mn content a spin-glass state is expected. In contrast, for GaN:Cr and GaN:V a ferromagnetic ordering is predicted for even higher concentrations of transition metals up to 25%. In the case of Fe, Co, or Ni doping a spin-glass ground state is expected. Interestingly, according to their band structure calculations, ferromagnetic ordering in *n*-type GaN:V seems to be possible, which is related to the partial filling of the antibonding *d*-states.

Many techniques were employed for the fabrication of GaN-based DMS, i.e., molecular beam epitaxy (MBE),[9,10] metal organic chemical vapor deposition (MOCVD),[11,12] ammonothermal technique,[13] or ion implantation.[14–16] The latter allows to incorporate impurity ions to concentrations exceeding the thermal-equilibrium solid solubility and gives freedom of choice of the materials to be implanted. Various groups reported on either ferromagnetic[11,12,14–16] or paramagnetic,[9] antiferromagnetic[13] or spin-glass[10] behavior. The origin of the ferromagnetism in GaN-based DMS is thus far from being understood. Hence, the question whether it is possible to fabricate homogeneous ferromagnetic layers without precipitation is of particular importance and still open.

For solving the problem of injection of the spin-polarized current into diluted magnetic GaN layers good ohmic contacts are necessary. The resistance of ohmic contacts to the *n*-type material is significantly lower than the contact resistance to the *p*-type GaN. Because of the wide band gap and strong Fermi level pinning[17] a large Schottky barrier in the case of *p*-type GaN is present. Thus, in spite of the fact that vanadium ions possess a magnetic moment smaller than that of manganese, *n*-type GaN:V might be of advantage for the preparation of ohmic contacts and electrical spin injection.

All these considerations encouraged us to investigate the magnetic properties of *n*-type GaN layers implanted with Mn, Cr, or V ions and compare them with the properties of *p*-type GaN layers implanted with Mn. In addition, composition profiles measured by secondary ion mass spectroscopy

[a]Electronic mail: v.guzenko@fz-juelich.de

 © 2004 American Institute of Physics

Downloaded 15 Dec 2006 to 134.94.122.39. Redistribution subject to AIP license or copyright, see http://jap.aip.org/jap/copyright.jsp

TABLE I. Sample overview.

Sample	Implant	Thickness (μm)		Dopant	
		Undoped	Doped	Element	Content (cm^{-3})
A1	Mn	3.0	1.5	Si	2×10^{17}
A2	Cr	3.0	1.5	Si	2×10^{17}
A3	V	3.0	1.5	Si	2×10^{17}
B1	Mn	1.0	1.0	Mg	2×10^{17}

(SIMS) and the microstructure of selected samples investigated by transmission electron microscopy (TEM) were also performed.

II. EXPERIMENTAL RESULTS

The GaN layers used in this study were grown by MOCVD on a (0001) sapphire substrate. Two types of doped GaN films were used: a 1.5 μm thick *n*-type layer, doped with Si to the concentration of 2×10^{17} cm^{-3} (samples $A1$–$A3$), and a 1.0 μm thick *p*-type GaN layer with a Mg doping concentration of 2×10^{17} cm^{-3} (sample $B1$). The *n*- and *p*-doped GaN layers are separated from the sapphire substrate by a 3 and 1 μm thick undoped GaN buffer layer, respectively. Mn^+, Cr^+, or V^+ ions were implanted perpendicular to the surface of the sample with an energy of 200 keV and a dose of 5×10^{16} cm^{-2}. During the implantation the samples were held at a temperature of 350 °C, in order to prevent amorphization. Subsequently, a rapid thermal annealing was performed in flowing N_2 atmosphere for 5 min at a constant temperature. In order to find out the optimum annealing procedure implanted samples were cut in pieces and each piece was annealed at a constant temperature in the range between 700 and 1050 °C. Cleaning of the samples in hydrochloric acid preceded the annealing step to remove residual unintentional ferromagnetic contaminations. Unless specified otherwise, we will focus below on the samples annealed at 700 °C, which are represented in Table I.

The magnetization of the samples was measured by a superconducting quantum interference device (SQUID) magnetometer (Quantum Design MPMS7) operating in the temperature range of 1.7–400 K and magnetic fields up to 7 T applied in the plane of the sample. Particular attention has been paid to enhance the sensitivity of the experimental setup and to reduce the systematic error due to the background signal from the sample holder. For this purpose a quartz glass rod with a diameter of 0.8 mm was designed. The rod was cleaned with hydrofluoric acid to remove residual ferromagnetic contaminations from the surface. The samples (3×10 mm^2) were fixed to the rod by a drop of glue, which was separately checked to be diamagnetic and was placed in the middle of the sample to avoid distortions of the measured SQUID signals.

In Fig. 1 the magnetization as a function of the magnetic field for Mn implanted samples $A1$ and $B1$, measured at the temperatures of 2, 10, and 100 K, are presented. The magnetization is presented in the dimensionless units of Bohr magnetons per atom, calculated according to the formula $m/(\mu_B AD)$, where m is the measured magnetic moment, A is the implanted area, D is the implantation dose, and μ_B is the value of one Bohr magneton. Because of the inhomogeneity of the implantation depth profile along the film thickness, this gives only a rough estimate of the polarization degree of the spins of the 3*d*-ions and is a good way to compare the samples with the different implants. The data show a typical paramagnetic behavior and can be fitted well by the Brillouin function for temperatures of 3, 10, and 100 K, assuming a spin $S=5/2$; a fit with $S=2$, corresponding to the Mn^{3+} ionization state, was not satisfactory. The diamagnetic background signal for all samples was subtracted by measuring the magnetization curve of the corresponding as-grown samples. No considerable difference between the samples initially *p*- and *n*-doped could be observed. A reasonable fit of the experimental data for the lowest temperature has been achieved only for an effective temperature T_{eff} slightly higher than the experimental one. At higher temperatures the difference between experimental and effective temperatures is negligible. Furthermore, the magnetization saturates with the magnetic field much more slowly than for the ferromagnetic GaMnAs (Ref. 1) and a discrepancy between the measured and calculated saturation magnetization was observed. The experimentally determined magnetization M at 2 K (symbols in Fig. 1, left axis) is lower by a factor of 0.22 in respect to the theoretically expected one M_{calc} (solid lines in Fig. 1, right axis). In the following, we denominate this factor by $x_{\mathrm{eff}}\equiv M/M_{\mathrm{calc}}$. The evaluation of the magnetization curves of the samples A1, A2, and A3 at 2 and 10 K reveals a similar behavior for the Cr($S=2$) and V($S=3/2$) implanted samples (Fig. 2). The measured saturation magnetization of

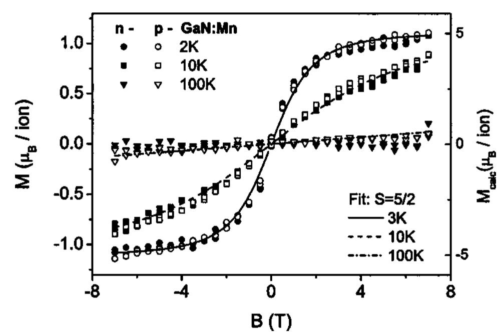

FIG. 1. Magnetization curves of the GaN:Mn samples $A1$ and $B1$ at 2, 10, and 100 K. Filled and open symbols represent experimental data for the samples $A1$ and $B1$, respectively. The lines display fits by the Brillouin function calculated for spin $S=5/2$ and effective temperatures 3, 10, and 100 K respectively. The left axis represents the experimental magnetization data in the units of Bohr magnetons per implanted ion. The right axis represents the calculated magnetization.

Downloaded 15 Dec 2006 to 134.94.122.39. Redistribution subject to AIP license or copyright, see http://jap.aip.org/jap/copyright.jsp

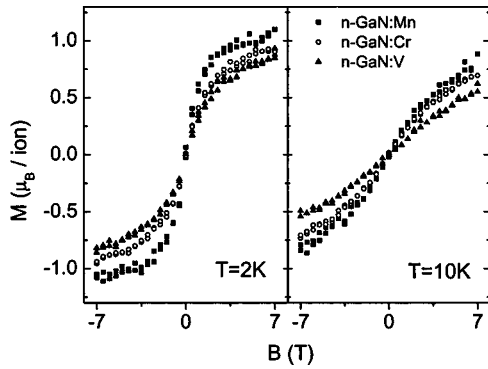

FIG. 2. Magnetization curves of GaN:X (X=Mn, Cr, or V) samples *A*1, *A*2, and *A*3, measured at 2 and 10 K.

these samples is lower in comparison with the Mn implanted sample, while the values of x_{eff} are higher: almost 0.28 at 2 K for the V implanted sample *A*3 and ≈0.23 for the Cr implanted sample *A*2.

An indication of the paramagnetic behavior can also be found in the temperature dependency of the magnetic moment of all GaN:X (X=Mn, Cr, or V) samples measured at a constant magnetic field of 50 mT. The experimental curves are shown in Fig. 3. All data can be fitted by the Curie-Weiss law $1/(T-\Theta)$, with the corresponding Curie-Weiss temperatures Θ having negative values, which is an indication of the antiferromagnetic coupling between implanted ions.

In order to better understand the origin of the paramagnetic behavior of the implanted GaN samples, their composition and crystalline structure has been investigated. In Fig. 4 SIMS depth profiles of as-implanted and annealed intrinsic GaN:Mn samples are presented. The stopping range of Mn ions is ≈220 nm (Fig. 4, inset). A significant difference in the Mn content of the as-implanted and the annealed samples can be observed only down to a depth of 90 nm. One can see that the maximum of the Mn concentration shifts towards the surface after annealing, while the impurity concentration remains unchanged at larger depth. The diffusion of the implanted ions can be attributed to the high density of point defects like vacancies, which arise after implantation mainly in the uppermost layer closer to the surface.

Additional information about the structural properties of implanted GaN is gained by transmission electron microscopy. The bright field image (Fig. 5) gives an overview of

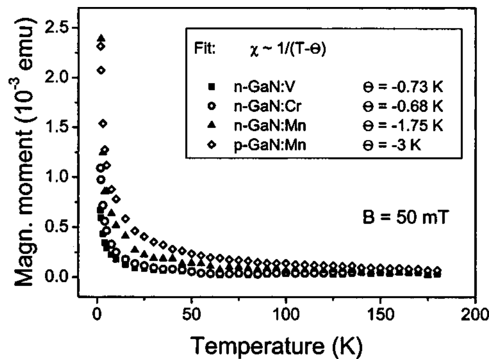

FIG. 3. Temperature dependence of the magnetization of all samples (*A*1–*A*3, *B*1) measured at a field of 50 mT.

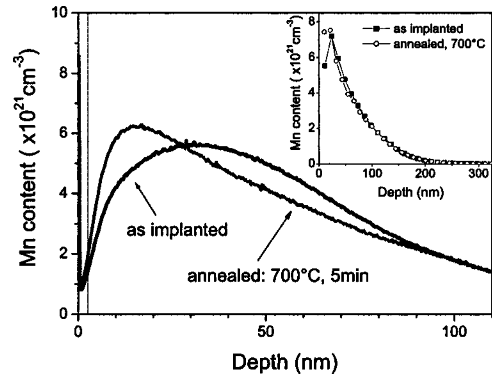

FIG. 4. Comparison of secondary ion mass spectra (SIMS) of intrinsic GaN:Mn layers as implanted and after the rapid thermal annealing at 700 °C for 5 min in flowing nitrogen atmosphere. The inset shows the depth profiles for the same samples taken over a larger depth range.

the implantation induced defect structure. Dark regions correspond to strain fields. Two regions of different contrast can be distinguished. Within the depth region from 200 to 280 nm a high density of small dislocation loops, about 2 nm in diameter, is observed in high-resolution micrographs (not shown here). The top layer extending over about 200 nm from the surface contains a Cr concentration gradient with a decrease of 5 at.% near the surface to less than 1 at.% at a depth of 150 nm according to energy dispersive x-ray analysis. The high-resolution electron micrograph shown in Fig. 6 reveals that besides planar defects consisting mainly of stacking faults (see arrow) numerous precipitates are present. These are identified by Moiré-contrasts of up to 5 nm in diameter superimposing the lattice fringe contrast of the GaN matrix. It can be concluded, that the precipitates are of crystalline nature. Although the crystalline phase of the precipitates could not be determined, they could be shown to be enriched with Cr by means of energy loss filtered imaging. Detailed results concerning this issue will be published elsewhere.

It is also important to mention that all our samples both initially *p*- and *n*-doped became extremely highly resistive or even insulating after ion implantation. This can be attributed

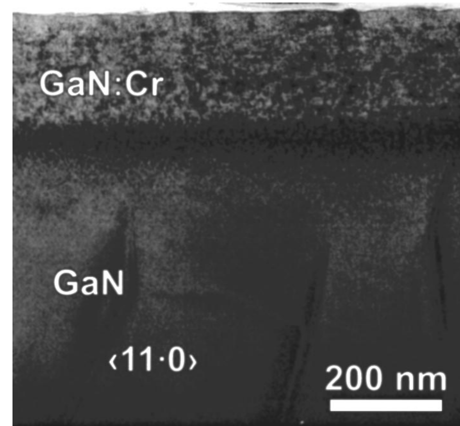

FIG. 5. TEM bright field image of a cross-sectional sample showing dark regions arising from strain fields of implantation-induced defects. Within the not-implanted region faint contrast lines arising from dislocations are revealed.

Downloaded 15 Dec 2006 to 134.94.122.39. Redistribution subject to AIP license or copyright, see http://jap.aip.org/jap/copyright.jsp

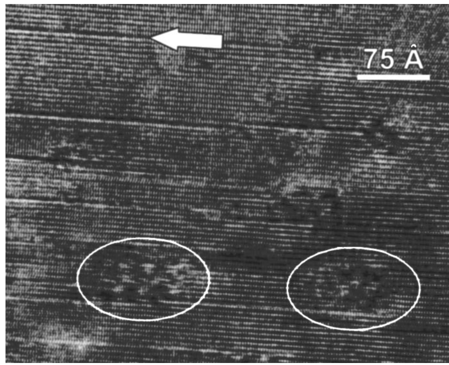

FIG. 6. High-resolution transmission electron micrograph of a GaN:Cr sample, annealed at 900 °C, in cross section. The implanted layer shows a high density of defects: stacking faults (shown by an arrow) in plane perpendicular to the *c*-axis and Moiré fringes (marked by ovals) can be clearly seen.

to deep electron traps, occurring due to the formation of complexes between the transition metal ions and native defects as well as due to radiation damage defects not involving transition metal ions.[18]

III. DISCUSSION

All investigated samples have shown a paramagnetic behavior. However, the saturation magnetization which is lower than the calculated one and the negative Curie-Weiss temperature are the indications of a weak antiferromagnetic coupling between implanted ions. A similar effect was observed by Graf *et al.*[9] and Zając *et al.*[13] in GaN:Mn samples with different Mn concentrations, grown by MBE and the ammonothermal technique, respectively. For highly diluted GaN:Mn, where the spatial separation of spins is large, the magnetization data could be described by the classical Brillouin function B_S. In samples with a high 3*d*-metal impurity content the magnetic ions are found closer to each other and can consequently interact stronger. This leads to the formation of pairs and/or larger clusters of antiferromagnetically ordered spins. For these samples an effective temperature T_{eff} and an effective Mn content Nx_{eff} with $x_{\text{eff}}<1$ can be introduced, so that the magnetization can be expressed by

$$M = Nx_{\text{eff}} g \mu_B S B_S(B, T_{\text{eff}}), \tag{1}$$

where N is the total number of the implanted ions, $g \approx 2$ is the Landé factor, and μ_B is the Bohr magneton. The antiferromagnetically coupled spins respond to the applied magnetic field less effectively than the noninteracting one, leading to an effective temperature T_{eff} larger than the experimental temperature T_{exp}. Moreover, the total spin of such clusters is zero or equal to the spin of the single ions, depending on the number of ions in a particular cluster. As a result, a lower saturation magnetization is measured, which can be expressed by lower concentration $(x_{\text{eff}}<1)$.

In our samples a high concentration of magnetic impurities is contained and so a coexistence of paramagnetic and antiferromagnetic behavior of implanted GaN layers was observed. The fit of the experimental magnetization data by a Brillouin function could be done with x_{eff} being noticeably lower than unity (see Table II). In addition, the effective

TABLE II. Effective parameters for the magnetization M.

Sample	$T_{\text{exp}}=2$ K		$T_{\text{exp}}=10$ K	
	x_{eff}	T_{eff} (K)	x_{eff}	T_{eff} (K)
*A*1	0.22	3	0.23	10
*A*2	0.23	3	0.25	10
*A*3	0.28	3	0.29	10
*B*1	0.22	3	0.23	10

temperature T_{eff} is slightly higher than the experimental one. It is remarkable that the value of x_{eff} reduces with an increasing number of *d*-electrons, i.e., ion spin. We attribute this to a stronger interaction between ions with increasing spin. Since the implanted ions couple antiferromagnetically, the response to the applied magnetic field is the highest for the V implanted sample and the lowest for the Mn implanted one. This is then reflected in the value of x_{eff}. At higher measurement temperatures the antiferromagnetic coupling between 3d-ions becomes weaker, which in turn results in an increase of x_{eff} (see Table II). An additional reason that accounts for the lowering of the saturation magnetization in our experiments is the sputtering of the samples during the implantation (sputtering yield is 5–9 atoms/ion,[19] which leads to a reduction of the number of implanted ions N. However, the effect of the sputtering on the value of the measured saturation magnetization does not exceed 3%.

The antiferromagnetic coupling of the implanted ions can have several reasons. The theoretical predictions of the ferromagnetic ordering in GaN:X (X=Mn, Cr, or V) are based on the assumption that a high density of delocalized valence band holes is provided, otherwise the antiferromagnetic (or spin glass) state is energetically preferred. Since all samples prepared in this study are highly resistive, i.e., the concentration of the free carriers is low, an antiferromagnetic, rather than a ferromagnetic, coupling between implanted ions is expected.

Furthermore, since the concentration of 3*d*-ions exceeds the solubility limit in GaN the formation of an antiferromagnetic secondary phase during the annealing procedure cannot be excluded. The presence of precipitates in the top layer was demonstrated by high-resolution TEM. However, detailed study of the crystalline structure as well as the chemical composition is necessary to draw conclusions concerning their magnetic properties.

IV. CONCLUSIONS

We have prepared GaN:X (X=Mn, Cr, or V) layers by means of ion implantation and subsequent annealing for 5 min in a flowing N_2 atmosphere at a constant temperature in the range between 700 and 1050 °C. Studies of the magnetic properties of these samples reveal paramagnetic behavior with an antiferromagnetic coupling between the 3*d*-metal ions. This behavior can be explained by the low concentration of the delocalized carriers necessary to mediate the ferromagnetism. Also formation of precipitates of antiferromagnetic secondary phase cannot be excluded. No indications of a ferromagnetic ordering of the implanted ions was found.

Downloaded 15 Dec 2006 to 134.94.122.39. Redistribution subject to AIP license or copyright, see http://jap.aip.org/jap/copyright.jsp

ACKNOWLEDGMENTS

We thank U. Zastrow (IPV, Research Centre Jülich) for the SIMS measurements. We thank Professor P. H. Dederichs, Dr. K. Sato, and Dr. P. Mavropoulos for fruitful discussions.

[1]H. Ohno, Science **281**, 951 (1998).
[2]G. Schmidt, D. Ferrand, L. W. Molenkamp, A. T. Filip, and B. J. van Wees, Phys. Rev. B **62**, R4790 (2000).
[3]T. Figielski and T. Wosinski, Physica E (Amsterdam) **9**, 295 (2001).
[4]B. Beschoten *et al.*, Phys. Rev. B **63**, 121202 (2001).
[5]S. Krishnamurthy, M. van Schilfgaarde, and N. Newman, Appl. Phys. Lett. **83**, 1761 (2003).
[6]T. Dietl, H. Ohno, F. Matsukura, J. Cibert, and D. Ferrand, Science **287**, 1019 (2000).
[7]K. Sato and H. Katayama-Yoshida, Jpn. J. Appl. Phys., Part 2 **40**, L485 (2001).
[8]K. Sato, H. Katayama-Yoshida, and P. H. Dederichs, J. Supercond. **16**, 31 (2003).
[9]T. Graf, M. Gjukic, M. Hermann, M. S. Brandt, M. Stutzmann, L. Görgens, J. B. Philipp, and O. Ambacher, J. Appl. Phys. **93**, 9697 (2003).
[10]S. Dhar, Appl. Phys. Lett. **82**, 2077 (2003).
[11]M. L. Reed, N. A. El-Masry, H. H. Stadelmaier, M. K. Ritums, M. J. Reed, C. A. Parker, J. C. Roberts, and S. M. Bedair, Appl. Phys. Lett. **79**, 3473 (2001).
[12]M. L. Reed, M. K. Ritums, H. H. Stadelmaier, M. J. Reed, C. A. Parker, S. M. Bedair, and N. A. El-Masry, Mater. Lett. **51**, 500 (2001).
[13]M. Zając, J. Gosk, M. Kaminska, A. Twardowski, T. Szyszko, and S. Podsiadlo, Appl. Phys. Lett. **79**, 2432 (2001).
[14]N. Theodoropoulou, A. F. Hebard, M. E. Overberg, C. R. Abernathy, S. J. Pearton, S. N. G. Chu, and R. G. Wilson, Appl. Phys. Lett. **78**, 3475 (2001).
[15]J. S. Lee, J. D. Lim, Z. G. Khim, Y. D. Park, S. J. Pearton, and S. N. G. Chu, J. Appl. Phys. **93**, 4512 (2003).
[16]J. M. Baik, J. K. Kim, H. W. Jang, Y. Shon, T. W. Kang, and J.-L. Lee, Phys. Status Solidi B **234**, 943 (2002).
[17]J. Rennie, M. Onomura, S.-Y. Nunoue, G.-I. Hatakoshi, H. Sugawara, and M. Ishikawa, J. Cryst. Growth **189-190**, 711 (1998).
[18]A. Y. Polyakov, N. B. Smirnov, A. V. Govorkov, N. V. Pashkova, A. A. Shlensky, S. J. Pearton, M. E. Overberg, C. R. Abernathy, J. M. Zavada, and R. G. Wilson, J. Appl. Phys. **93**, 5388 (2003).
[19]A. J. Steckla and I. Chyr, J. Vac. Sci. Technol. B **17**, 362 (1999).

Downloaded 15 Dec 2006 to 134.94.122.39. Redistribution subject to AIP license or copyright, see http://jap.aip.org/jap/copyright.jsp